Anticausal behavior in the imaging of a moving object: The implications for high-speed photography

Kenneth L. Sala*
Division of Physics, National Research Council of Canada, Ottawa, Ontario K1A OR6, Canada
(Received 21 August 1978)

An analysis of the temporal behavior of the image of a moving object in a simple imaging system is presented which explicitly takes into account the finite transit time of the light propagating from the object to the image plane. This analysis, which places no restrictions on the magnification of the imaging system or on the spatial shape or extent of the object, uncovers a number of novel and highly unorthodox phenomena hitherto unforeseen. Of particular significance, in the case where the object velocity v_o and the magnification M satisfy $(M+1)v_o/c > 1$, is the finding that a single object gives rise to two simultaneous images which move antiparallel to one another away from a common point in the image plane. One of these images displays a normal, forward time dependence, while the other image exhibits a time-reversal character resulting in the anticausality in the observed temporal behavior of the object and of time-dependent or causal events associated with it. The theory is developed to include the imaging of arbitrary, three-dimensional objects. The important case where the object is stationary but has a time-dependent intensity distribution is also examined and it is shown, in this case as well, that anticausal behavior can be observed in the image plane under quite general conditions. The ramifications of this work for high-speed photography in general are discussed, and numerous illustrations are given of the image behavior in time for moving objects of simple geometrical shapes.

I. INTRODUCTION

The development of the optical-Kerr-effect shutter[1] gated by ultrashort laser pulses has resulted in the extension of high-speed, two-dimensional photography to the picosecond regime.[2-8] Stop-motion photography of single ultrashort light pulses in flight has been performed[5,7,8] using an optical-Kerr-effect shutter switched by picosecond mode locked pulses from a Nd:glass laser. In addition, the development of the picosecond optical streak camera[9-11] has presented an alternate high-speed photographic technique enabling a one-dimensional recording continuous on a picosecond time scale. This new found ability to photographically time resolve relativistic phenomena such as a travelling-light pulse necessitates a careful reexamination of the details of image formation paying close attention to the effects resulting from finite differences in transit times from the object to the image plane.[5] Indeed, a general interest in the subject of the instantaneous visual appearance of a rapidly moving object has existed since the original publications by Penrose[12] and Terrell[13] in 1959 on this topic.[14] Their work plus that of a number of other authors since[15] have made it clear that what is "seen" by a single observer at an instant in time is markedly different and more complex than the simple Lorentz contraction usually ascribed to a relativistic body. Work on this subject, however, has been invariably cast in the mathematical framework of Lorentz transformations and relativistic kinematics. More importantly, from the viewpoint of relevance to practical high-speed photographic systems, the question of the critical role played by the imaging system has either been ignored completely or else implicitly avoided by effectively assuming the magnification to be $\ll 1$ (e.g., the human eye as "observer" of distant objects).

The present paper considers a simple imaging system and the resulting image behavior in time when the finite transit time of light travelling from the object to the image plane is explicitly included in the analysis. No restrictions are placed on the dimensions or the magnification M of the imaging system or upon the spatial extent of the object. This analysis, which is presented entirely in the language of geometrical optics, reveals a number of novel and rather unorthodox phenomena which would not be possible if a negligibly small magnification were assumed. A principal finding, in the case where the object velocity v_0 and the magnification M satisfy $(M+1)v_0/c > 1$, is that the single object gives rise to two simultaneous images moving antiparallel away from each other in the image plane. While one of these images possesses a normal, forward time-dependent nature, the other image exhibits a time-reversal character leading to the anticausality both in the observed temporal behavior of the object and in that of time-dependent or causal events associated with the object. The analysis begins with the simplest case of a point source object moving with a constant velocity and is then generalized in steps to include two- and then fully three-dimensional objects. The case of

a stationary object having a time-dependent intensity distribution is also discussed and shown to likewise possess a potential for exhibiting anticausality in the image's temporal behavior. Numerous illustrations are given of the image behavior in time for moving objects of well-defined, simple geometrical shapes and a discussion is given of some of the implications of these findings for high-speed photography in general.

II. IMAGE OF A MOVING POINT SOURCE OBJECT

The imaging system is shown schematically in Fig. 1. The point-source object travels along the x_0 axis in the object plane with a constant velocity $v_0 > 0$, while the image of the point source travels along the x axis in the image plane. For convenience, the x_0 and x axes have been chosen to run antiparallel so that corresponding object and image points carry the same sign. The origin of each axis lies at its intersection with the optical axis of the lens L. The simple lens L is assumed to be a perfect, thin lens and the imaging system characterized by a "static," positive magnification $M = d/d_0$. For the purposes of calculating optical path lengths from the object to the image, Fermat's theorem ensures that the perfect, thin-lens system of Fig. 1 is formally equivalent to a pinhole imaging system with identical object and image plane spacings.

The position of the point source object at time t is given by its equation of motion

$$x_0(t) = v_0 t + v_0 s_0/c\,, \tag{1}$$

where $s_0 = d_0 + d = (M+1)d/M$ is the object to image-plane spacing, and the constant $v_0 s_0/c$ conveniently ensures that an image of the object appears at $x = 0$ at $t = 0$. For the perfect, thin lens, the optical path length from $x_0 = x/M$ to x is given by

$$s(x) = (M+1)(d^2 + x^2)^{1/2}/M = (M+1)d/M\cos\phi\,, \tag{2}$$

where the angle ϕ $(-\pi/2 \leq \phi \leq \pi/2)$, shown in Fig. 1, is defined by $\tan\phi = x/d$. The transit time of the light travelling from x/M to x is simply $\tau(x) = s(x)/c$.

The position of the point image at time t is determined by the position of the object at the time $t - \tau(x)$, i.e.,

$$x(t) = Mx_0[t - \tau(x)]\,. \tag{3}$$

Combining these three equations defines $t = t(x)$ directly as

$$Mv_0 t = x + \beta_M[(d^2 + x^2)^{1/2} - d]\,, \tag{4}$$

where

$$\beta_M = (M+1)v_0/c = (M+1)\beta_0\,. \tag{5}$$

Note that this parameter can be ≥ 1, unlike the usual relativistic parameter $\beta_0 = v_0/c < 1$.

The calculations to be presented here and throughout this paper are considerably simplified by the introduction of the dimensionless position, time, and velocity parameters

$$X \equiv x/d,\quad T \equiv Mv_0 t/d,\quad V \equiv v/Mv_0\,, \tag{6}$$

where $v = dx/dt$ is the instantaneous velocity of the point image. It follows immediately upon differentiation of Eq. (4) that

$$V = \frac{dX}{dT} = (1 + \beta_M \sin\phi)^{-1} \tag{7}$$

with $\sin\phi = X/(1+X^2)^{1/2}$. Equation (4) also yields the quadratic equation in X, determining the image motion $X(T)$,

$$(\beta_M^2 - 1)X^2 + 2(T + \beta_M)X - (T^2 + 2\beta_M T) = 0\,. \tag{8}$$

Either of these last two equations clearly reveals that the form of the image motion is uniquely and solely determined by the parameter β_M.

The precise nature of the image behavior, according to Eq. (8), depends critically upon whether the value of β_M is <1, $=1$, or >1, and care must be exercised in choosing the solution(s) $X(T)$ from Eq. (8) in each of these cases. Correctness is assured in each case by referring back to the unambiguous Eq. (4) giving $T = T(X)$. Thus, when $\beta_M < 1$, T is a strictly monotonic function of X so that the solution $X(T)$ given by Eq. (8) must be for $\beta_M < 1$

$$X(T) = (1 - \beta_M^2)^{-1}[T + \beta_M - \beta_M(T^2 + 2\beta_M T + 1)^{1/2}]\,, \quad -\infty < T < \infty \tag{9}$$

with the choice of the correct root from Eq. (8) governed by the requirement that it satisfy the

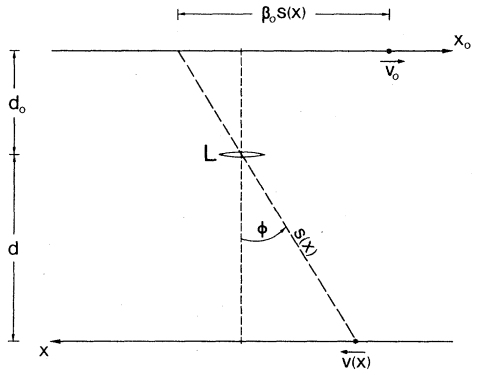

FIG. 1. Simple imaging system for the moving-point-source object. Note the nonconjugate, instantaneous object and image positions.

"boundary" condition $X(T=0)=0$ prescribed by Eq. (1). For the special case of $\beta_M=1$, the dependence of $T(X)$ is asymptotic to the "initial" values X_{int} and T_{int} (defined below), and the unique solution given by Eq. (8) is for $\beta_M=1$

$$X(T)=\tfrac{1}{2}[1+(1+T)^{-1}]T\,,\quad T\geq T_{\text{int}}\,. \tag{10}$$

Finally, since for $\beta_M>1$ the dependence of $T(X)$ is parabolic about the turning point X_{int} and T_{int}, the solution $X(T)$ consists of both the roots to Eq. (8), i.e., for $\beta_M>1$

$$X(T)=X_{\pm}(T)$$
$$=(\beta_M^2-1)^{-1}[-T-\beta_M\pm\beta_M(T^2+2\beta_M T+1)^{1/2}]\,,$$
$$T\geq T_{\text{int}}\,. \tag{11}$$

For $\beta_M\geq 1$, the initial values X_{int} and T_{int} are simply those values of X and T at which $|V|\to\infty$ and are given by[16]

$$X_{\text{int}}=-(\beta_M^2-1)^{-1/2},\quad T_{\text{int}}=(\beta_M^2-1)^{1/2}-\beta_M\,(\beta_M\geq 1), \tag{12}$$

with the values $T_{\text{int}}=-1$ and $X_{\text{int}}=-\infty$ for the special case of $\beta_M=1$.

Figure 2(a) shows the point-image motion $X(T)$ for each of the cases $\beta_M<1$, $\beta_M=1$, and $\beta_M>1$, while the dependence of the instantaneous image velocity $V(X)$ is shown in Fig. 2(b) for the same β_M values. Also shown in Fig. 2(a) is the limiting case of $\beta_M\ll 1$, for which $X=T$ and $V=1$ (i.e., $x=Mv_0t$ and $v=Mv_0$). Noteworthy is the fact that, when $\beta_M\geq 1$, the image is present only for times T later than T_{int} with no image being present anywhere in the image plane for times earlier than T_{int}. But clearly, the most striking anomaly portrayed in Fig. 2 is the existence, in the case where $\beta_M>1$, of two images simultaneously present in the image plane which travel antiparallel to one another from a common origin at X_{int}. That image having $V>0$ and described by the $X_+(T)$ solution of Eq. (11) is referred to as the normal or causal image. The other image characterized by $V<0$ and given by

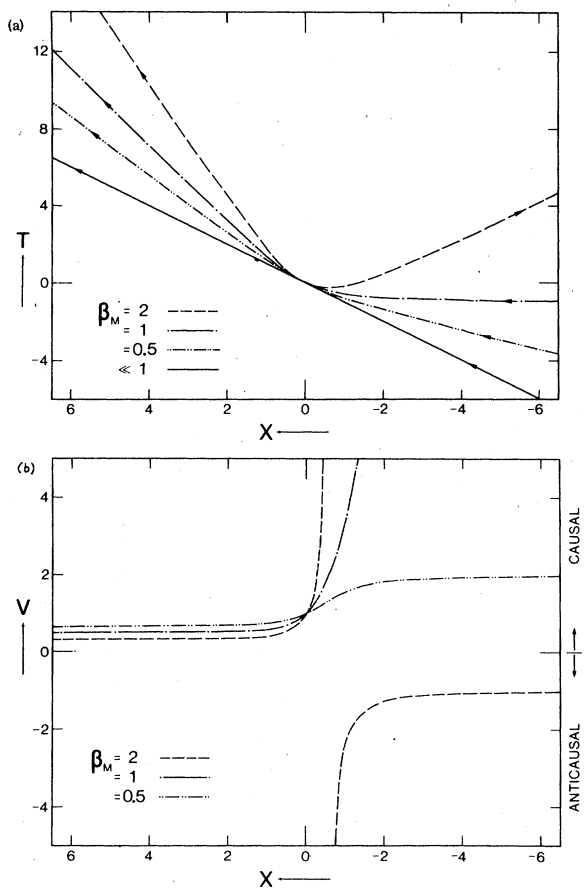

FIG. 2. (a) Motion of the image of the point-source object and, (b) instantaneous velocity of the point image, for $\beta_M<1$, $=1$, and >1.

$X_-(T)$ from Eq. (11) is referred to as the time-reversed or anticausal image.

To make clearer the physical basis underlying the rather unorthodox behavior illustrated in Fig. 2, it is helpful, using the identity $dx=(d/\cos^2\phi)d\phi$, to rewrite the expression for the instantaneous image velocity in the form

$$v(x)=\frac{dx}{dt}=\frac{(d/\cos^2\phi)d\phi}{(d/Mv_0\cos^2\phi)d\phi+[d(M+1)\sin\phi/M\cos^2\phi]\,d\phi/c}\,. \tag{13}$$

Expressed in this way, it is seen that the incremental time dt required for the image to move from x to $x+dx$ is composed of two contributions. The first,

$$dt_0=(d/Mv_0\cos^2\phi)d\phi=dx_0/v_0=dx/Mv_0 \tag{14}$$

is simply the time required for the object to move from $x_0=x/M$ to $x_0+dx_0=(x+dx)/M$, while the second contribution to dt is

$$d\tau=[d(M+1)\sin\phi/M\cos^2\phi]d\phi/c=ds(x)/c \tag{15}$$

and gives the change in the transit time from $x_0=x/M$ to x compared with that from $x_0+dx_0=(x+dx)/M$ to $x+dx$. The ratio of the two contributions is $d\tau/dt_0=\beta_M\sin\phi$, and it is the variation of this ratio with position x which principally defines the characteristics of the image motion [note Fig. 2(b) and the relation $d\tau/dt_0=(1-V)/V$]. Spec-

ifically, two completely different types of temporal behavior occur in the image according to whether $d\tau/dt_0$ is >-1 or <-1, the latter inequality being possible only when $\beta_M > 1$. The case of $\beta_M < 1$ is the most straightforward in that $d\tau/dt_0$ is >-1 for all values of X. This, in effect guarantees that the light reaching the image plane always does so in exactly the same temporal order as originally emitted from the object and so $V > 0$ everywhere. Of course, although the temporal ordering is preserved, absolute temporal differences are not since the dependence of τ upon x is highly nonlinear. Hence the image motion $X(T)$ is also nonlinear, becoming linear only in the limit of $\beta_M \ll 1$. The special case of $\beta_M = 1$ represents a "crossover" value for which $V(X)$ first exhibits a singularity (asymtotically as $X \to -\infty$). The value of $d\tau/dt_0$ is only very slightly >-1 in the region $X \ll -1$ with the result that the image appears very nearly simultaneously along the entire length of the negative x axis. Nevertheless, $d\tau/dt_0$ is strictly >-1 everywhere (V always >0) so that no time reversal in the imaged light occurs in the case of $\beta_M = 1$. When $\beta_M > 1$, however, the ratio $d\tau/dt_0$ will be <-1 in the range $X < X_{\text{int}}$. Thus, in this range, the "foreshortening" in the transit time as the object moves from $x_0 = x/M$ (where $x/d < X_{\text{int}}$) to $x_0 + dx_0$ (where $dx_0 > 0$) exceeds in magnitude the translational time $dt_0 = dx_0/v_0$ with the result that the image at $x + dx = M(x_0 + dx_0)$ appears *earlier* than that at $x = Mx_0$, even though the light from $x_0 + dx_0$ was in fact emitted *later* than that from x_0. In short, the image motion is time reversed or anticausal in the range $X < X_{\text{int}}$. In the range $X > X_{\text{int}}$, on the other hand, $d\tau/dt_0 > -1$ and so the image motion is temporally normal or causal.

III. IMAGING OF A ONE-DIMENSIONAL OBJECT

The analysis just given for the imaging of a point-source object served to make clear the nonlinear nature of the image motion and to establish the existence of the two coexisting causal and anticausal images in the case where $\beta_M > 1$. To carry this analysis further and to introduce the concept of a "local magnification", this section examines the motion of a simple one-dimensional object (i.e., having a depth and height $\ll d/M$). Specifically, the object described is a one-dimensional "measuring stick" of length[17] l_0 and is represented here by five equally spaced point objects which move according to

$$x_{0n} = v_0 t + (\beta_M''/M)(d^2 + \tfrac{1}{4}M^2 l_0^2)^{1/2} + \tfrac{1}{4}(3-n)l_0, \qquad (16)$$

$$n = 1 \text{ to } 5.$$

The front and end of the measuring stick are represented by the markers $n = 1$ and $n = 5$, respectively, while the $n = 2$, 3, and 4 points locate the $\frac{1}{4}l_0$, $\frac{1}{2}l_0$, and $\frac{3}{4}l_0$ markers, respectively. The constant of motion in Eq. (16) is included to conveniently ensure that an image of the object will be centered about the optic axis at $t = 0$. Using Eqs. (2) and (3) and the dimensionless parameters given in Eq. (6), the equation determining the motion of the corresponding image points X_1 to X_5 is

$$X_n = T - \beta_M(1 + X_n^2)^{1/2} + \beta_M(1 + \tfrac{1}{4}L_0^2)^{1/2} + \tfrac{1}{4}(3-n)L_0, \qquad (17)$$

$$n = 1 \text{ to } 5,$$

where $L_0 = Ml_0/d$ is the dimensionless length parameter. The particular solution(s) $X_n(T)$ are found from Eq. (17) according to the value of β_M being <1, $=1$, or >1 as given in the previous section.

Figure 3 shows the motion of the one-dimensional measuring stick having a length $L_0 = 1$ for each of the cases of $\beta_M < 1$, $\beta_M = 1$, and $\beta_M > 1$. The continuous motion of each of the five markers X_n is shown as well as the instantaneous appearance of the measuring stick at a series of discrete times T. Clearly, at no time does the image of the measuring stick correspond to a uniformly Lorentz contracted rod. Rather, the overall length of the image varies continuously in time and, moreover, the spacings between the internal markers within the image differ at any given instant. Hence, even though in all cases the overall length of that image centered about the optic axis at $T = 0$ is exactly equal to $L_0 = 1$, this particular image is nonetheless unfaithful since there exists a marked degree of internal distortion within the image. A strictly faithful image, i.e., one which is distortion-free although not necessarily having the correct overall length, is only obtained[18] in the limit of $L_0 \ll 1$ or $\beta_M \ll 1$ or both. Nevertheless, for the purpose of obtaining the best approximation to a faithful image in a high-speed photographic system with β_M and L_0 finite, the image must be recorded precisely at that instant when it lies centered about the optic axis. Note that special care must be taken in the case where $\beta_M > 1$, Fig. 3(c), to distinguish between the causal and anticausal images in interpreting the instantaneous image during that interval of time after the front of the measuring stick first appears and before the end of the stick is visible.

As Fig. 3 illustrates, the degree of distortion within the image at any time varies continuously with position X. One can thus speak of a "local" or differential magnification $\Pi_x(X)$, which is defined to be the instantaneous value of the ratio dx/dx_0, where dx is the size of the image at X of an infinitesimally small moving object of length dx_0. Since this is formally equivalent to letting dx be the distance travelled in the time dt by the image of a

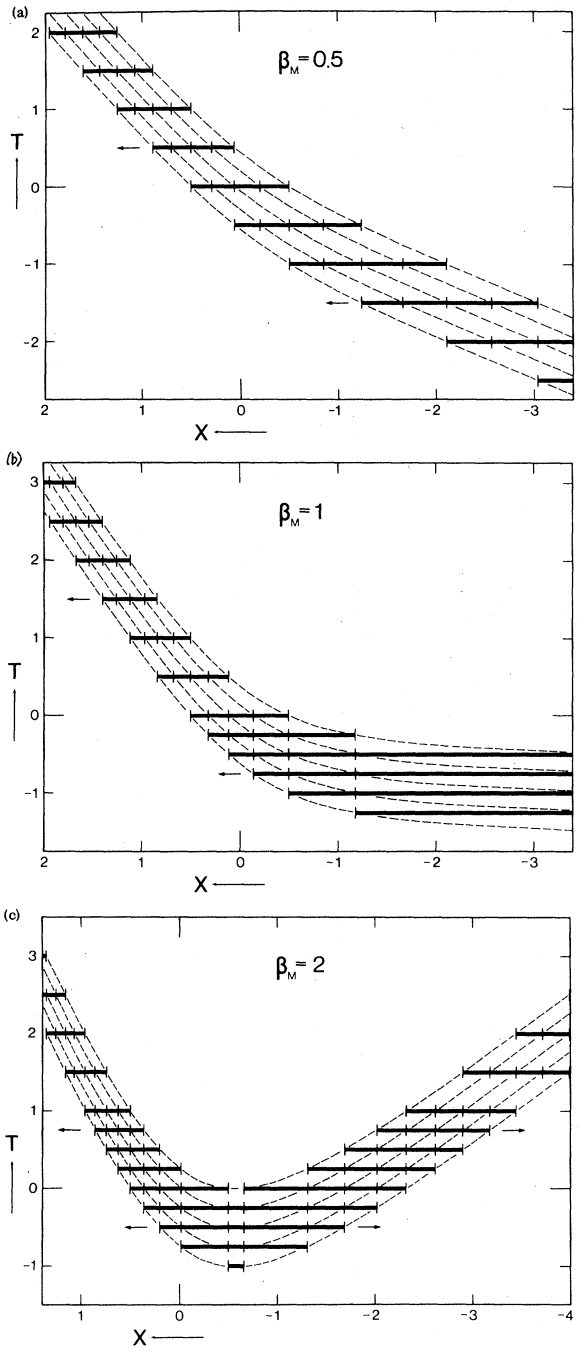

FIG. 3. Image of a one-dimensional measuring stick of length $L_0=1$. (a) $\beta_M<1$, (b) $\beta_M=1$, and (c) $\beta_M>1$.

moving point source object, $dx=vdt$ (and $dx_0=v_0dt$), then $\Pi_x(X)$ is simply the ratio v/v_0 given by

$$\Pi_x(X)=MV(X)=M/(1+\beta_M\sin\phi)\,. \tag{18}$$

Alternatively, exactly the same result may be derived with the aid of the measuring stick model of this section by letting $l_0\to dl_0$ in the knowledge that, by definition, $x_5\to x_1+\Pi_x(x_1)l_0$ in this limit. The overall or "gross" magnification in the image between any two points x_1 and x_2 is found by simply integrating $\Pi_x(X)$ from x_1 to x_2 and then dividing by $|x_1-x_2|$, taking care, in the case where $\beta_M>1$, to ensure that both x_1 and x_2 lie in either the causal or the anticausal image, but never one in each.

This simple $\Pi_x(X)=MV(X)$ relationship is, in turn, the basis of a simple but important relationship between the temporal "length" or duration of the object and that of the image. The temporal duration (or "time of passage") of the measuring stick as measured in the object plane is simply l_0/v_0. In the image plane, the temporal width of the image of the measuring stick when measured at the point X is given by

$$\Delta t=\int_{t(X_1=X)}^{t(X_5=X)}dt=\int_{x_{01}}^{x_{05}}v^{-1}\frac{dx}{dx_0}\,dx_0\,, \tag{19}$$

which, with $dx/dx_0=\Pi_x(x)=v/v_0$, gives the result

$$\Delta t=v_0^{-1}\int_{x_{01}}^{x_{05}}dx_0=l_0/v_0\,, \tag{20}$$

showing that the temporal duration of the measuring stick is exactly the same in both the object and image planes and, furthermore, is independent of the observer's position in the image plane. Derived in the completely general manner as above, this result is in fact seen to be a general theorem valid for arbitrary objects with x_{01} and x_{05} taken to represent the time "markers" for any convenient measure of the object's temporal length (e.g., the FWHM intensity points of an optical pulse). This finding rules out the possibility of ever generating or measuring times much shorter than Δt by, in some fashion, simply exploiting the "enhancement" of the instantaneous image velocity in that region where $V\gg1$.

IV. IMAGING OF A TWO-DIMENSIONAL OBJECT

Figure 4 illustrates schematically the imaging system, where it is noted that both the x and y axes are chosen to run antiparallel to the x_0 and y_0

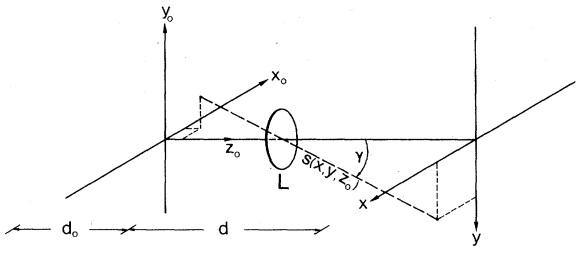

FIG. 4. Simple imaging system for two- and three-dimensional objects.

axes, respectively. In this section, it is assumed that the object is strictly two-dimensional and lies in the $z_0 = 0$ plane. Then, with $I_0(x_0, y_0, t)$ representing the instantaneous intensity distribution in the object plane ($z_0 = 0$), the intensity distribution in the image at time t is given by

$$I_i(x, y, t) = K_2 I_0(x/M, y/M, t - \tau(x, y)) , \qquad (21)$$

where $\tau(x, y) = s(x, y)/c$ is the transit time from $(x_0 = x/M, y_0 = y/M, z_0 = 0)$ to (x, y) with

$$s(x, y) = (d^2 + x^2 + y^2)^{1/2}(M+1)/M = d(M+1)/(M\cos\gamma) , \qquad (22)$$

where the angle γ $(0 \leq \gamma \leq \pi/2)$, shown in Fig. 4, is defined by $\tan\gamma = (x^2 + y^2)^{1/2}/d$. The constant K_2 in Eq. (21) is a lumped transmission coefficient intended to implicitly account for a variety of loss factors (aperturing, scattering, reflections, ...) which, although they may alter the relative distribution in intensity within the instantaneous image, do not affect either its spatial profile or extent.[19] The dimensions of I_0 are those of a power density (energy area^{-1} time^{-1}), while K_2 has the units of time.

Figure 5 illustrates the instantaneous appearance of the image at a series of discrete, sequential times for a square, two-dimensional object[17] [with diagonals as shown "at rest" in Fig. 5(a)] for each of the cases of $\beta_M < 1$, $\beta_M = 1$, and $\beta_M > 1$. The side length of the square object has the value $L_0 = Ml_0/d = 1$ for Fig. 5, and the image is described entirely in terms of the dimensionless "coordinates" $X = x/d$, $Y = y/d$, and $T = Mv_0 t/d$. These images were calculated directly from Eq. (21) with the object described as a sum of appropriate Dirac δ functions specifying the positions of the boundaries and diagonals of the square. A constant of motion (i.e., the T origin) was included which ensured that, for all values of β_M, the boundary points $Y = 0$ in the (causal) image at $T = 0$ lay centered about the optical axis. Clearly, at no time does the image faithfully "reproduce" the object and, indeed, at certain instants, bears rather little apparent resemblence to it. The case of $\beta_M > 1$ is again particularly noteworthy with the appearance, ultimately, of two distinct, two-dimensional images which travel away from each other from points along the "initial line" $X_{\text{int}} = -(1 + Y^2)^{1/2}/(\beta_M^2 - 1)^{1/2}$. The anticausal image, in the case where $\beta_M > 1$, of the two-dimensional object exhibits a rather peculiar feature unique to it alone. Thus, the causal images $(V > 0)$ in all cases are normal in that, as usual, both the x and y directions in the object appear inverted in the image. In the anticausal image, however, only the y direction is inverted with the x direction in the image remaining absolutely paral-

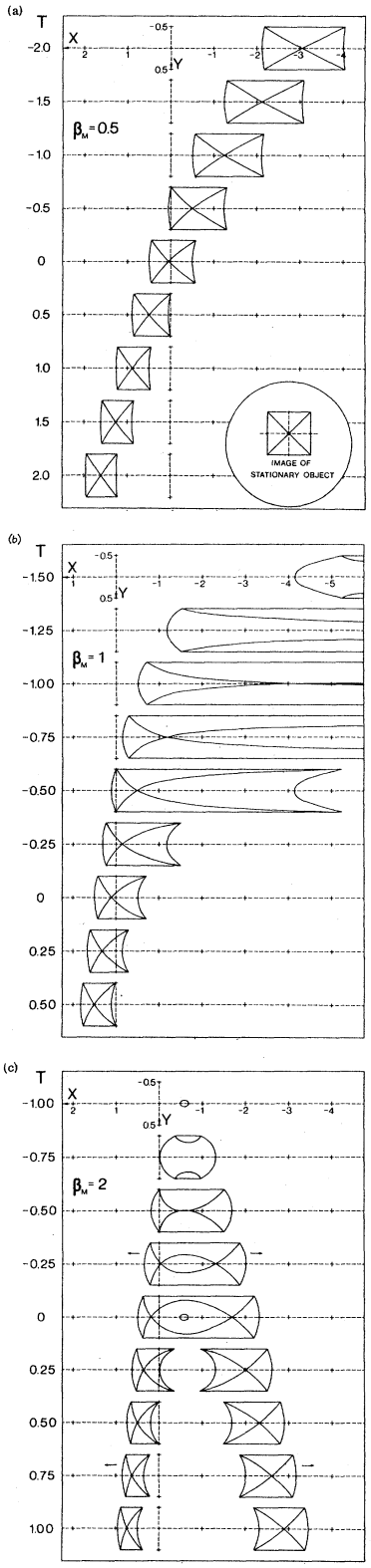

FIG. 5. Sequential, framed images of a travelling, square object with sides of length $L_0 = 1$. (a) $\beta_M < 1$, (b) $\beta_M = 1$, and (c) $\beta_M > 1$.

lel to that in the object. This "semi-inverted" characteristic of the anticausal image may be expected to produce, in its own right, bizarre and potentially confusing images. Also note that, for all of the images, the magnification parameter M remains as a "good" parameter for variations in the y direction, i.e., points in the object with a separation in their y_0 coordinates of Δy_0 appear in the image with a separation of $\Delta y = M\Delta y_0$. However, the local magnification along the x direction, $\Pi_x(x)$, varies markedly and so lengths in the object will generally transform into lengths in the image which depend quadratically upon M and the integrated Π_x.

The use of the term "anticausal" to describe the $V<0$ image in the case where $\beta_M>1$ refers to more than just the retromotion of the whole object. Any sequence of events occurring within the object as it moves along are also observed in a time-reversed order so that "cause followed by effect" in the object is observed as "effect followed by cause" in the image. To underline this time-reversed, anticausal characteristic, Fig. 6 illustrates the motion of a simple clock giving the "hours" and "minutes." Solely for convenience, the size of the clock face has been deliberately chosen to be small ($\ll d/M$) so that, upon enlargement, it may be seen essentially as undistorted (this does *not* affect the observation of time reversal). In Fig. 6, the length of one "hour" as measured by the clock has been chosen to correspond to the time it takes the clock to travel a distance $0.5d_0$ in the object plane. The image of the clock with $V<0$ in Fig. 6 is clearly seen to be that of a clock running backwards in time.

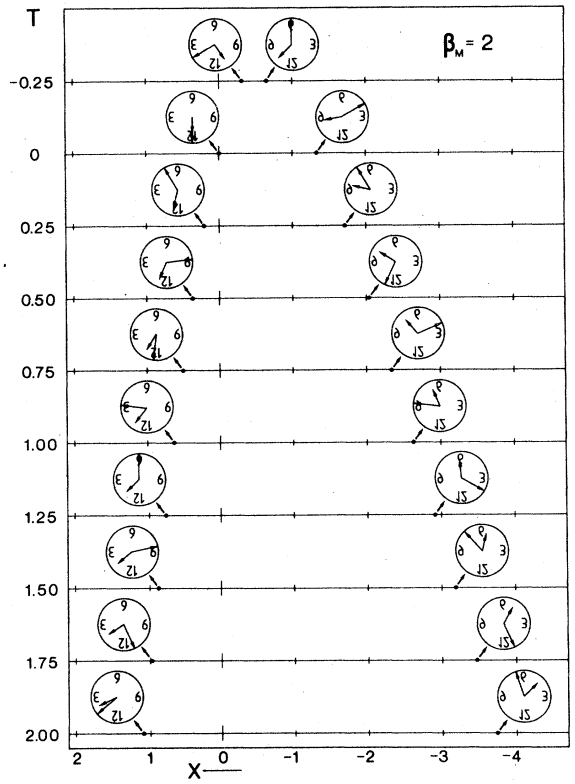

FIG. 6. Image of a travelling "clock" with $\beta_M>1$. The clock faces are shown enlarged.

V. IMAGING OF A THREE-DIMENSIONAL OBJECT

To finally extend this phenomenological formalism to include the imaging of an arbitrary, three-dimensional object, an assumption is first introduced which helps to make this extension straightforward. Specifically, it is assumed that the depth of field limits for the imaging system (Fig. 4) are greater than the spatial extent of the object along the (optic) z_0 axis. This assumption amounts to saying that all parts of the object can be brought to a sharp focus by the lens in the image plane $z=0$. More precisely, allowing explicitly for perspective in the imaging, all those points in the object which lie along the line $[x_0 = x/M_e(z_0), y_0 = y/M_e(z_0), z_0]$ are imaged onto the point (x, y) in the image plane, where

$$M_e(z_0) = M/[1-(Mz_0/d)] \tag{23}$$

is the z_0 dependent, "effective" magnification [$M = M_e(z_0=0) = d/d_0$ is the "principal" magnification from the $z_0=0$ object plane to the image]. Thus, the instantaneous image intensity distribution may be expressed as, with $Z_0 = z_0/d_0$,

$$I_i(x,y,t) = K_3 \int_{-\infty}^{\infty} I_0 \{x/M_e(z_0), y/M_e(z_0), z_0, t-\tau(x,y,z_0)\}\, dZ_0\,, \tag{24}$$

where $\tau(x,y,z_0) = s(x,y,z_0)/c$ is the transit time from the point $[x_0 = x/M_e(z_0), y/M_e(z_0)z_0]$ to $(x, y, z=0)$ with

$$s(x,y,z_0) = (d^2+x^2+y^2)^{1/2}[1+M_e^{-1}(z_0)] = \{1-[Mz_0/(M+1)d]\}\, s(x,y)\,, \tag{25}$$

where $s(x,y) = s(x,y,z_0=0)$ is given by Eq. (22). The $\pm\infty$ limits of integration in Eq. (24) are admissible under the assumption that the object lies entirely within the depth of field limits of the imaging system. The intensity distribution of the object is $I_0(x_0, y_0, z_0, t)$, in units of power area^{-1} and

represents the power radiated or scattered from the plane of thickness dz_0 centered at z_0. The constant K_3, with the units of time, is a lumped transmission coefficient representing the various losses in the imaging.[19] Note that Eq. (24) implicitly assumes the object to be optically transparent—an opaque object would require using only the minimum value of $s(x, y, z_0)$ at each point in the image plane.

Figure 7 shows, for a sequence of discrete times T, the instantaneous framed images for an object which is a simple cube[17] of side l_0 travelling parallel to the x_0 axis with a velocity $v_0 > 0$ and which has that face closest to the lens lying in the plane $z_0 = 0$. The value $L_0 = Ml_0/d = 1$ has been adopted in calculating Fig. 7. Figure 7(a) shows the usual image behavior when $\beta_M \ll 1$, while Figs. 7(b) and 7(c) show the image behavior for $\beta_M < 1$ and $\beta_M > 1$, respectively. A constant of motion has been included such that, at $T = 0$, the midpoints of the front face of the cube in the causal image lie centered at $X = \pm 0.5$ about the optical axis. The existence of a finite depth for a three-dimensional object is seen to further add to the overall distortion in the image. Thus, for example, the images seen at the times $T = -0.75$ and 0.25 in the case of $\beta_M = 2$ in Fig. 7(c) can certainly be said to bear almost no resemblence to the cubic object they in fact portray.

An essential point to note concerning the imaging of a three-dimensional object is that, in order to calculate the instantaneous image, it is necessary to specify the values of β_0 and of M separately and not just simply the single combined parameter $\beta_M = (M+1)\beta_0$ as was the case for the two- and one-dimensional objects (in Fig. 7, M has been kept constant and only β_0 varied). The intrinsic reason behind this is the fact that, for a three-dimensional object, the parameter M, and hence the parameter β_M, are no longer, strictly speaking, "good" parameters which characterize the entire object. Rather, because of imaging perspective and the "effective" magnification $M_e = M/[1 - (Mz_0/d)]$, one must also speak of an "effective" $\beta_M^e = (M_e + 1)\beta_0$ with $\beta_M = \beta_M^e(z_0 = 0)$. A close examination of Figs. 7(b) and 7(c) reveals that the amount of distortion is considerably less in the back face of the cube than in the front face, reflecting the fact β_M^e is less for the back face [note, however, that β_0, M, and L_0 were chosen such that β_M^e is <1 for the entire object in Fig. 7(b) and β_M^e is >1 for all parts of the object in Fig. 7(c)]. Thus, for a three-dimensional object, to specify a value of $\beta_M = 1$ would be somewhat misleading since a specific value of β_M applies strictly to only a single z_0 plane in the object. However, it is possible for the cubic object to have a value of $\beta_M > 1$ such that the effective val-

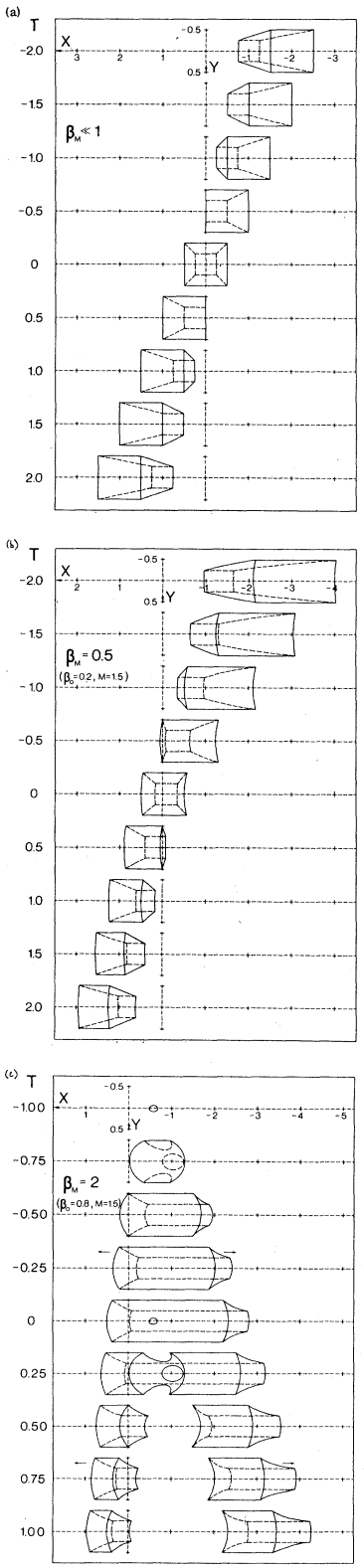

FIG. 7. Sequential, framed images of a travelling cube of side length $L_0 = 1$. (a) $\beta_M \ll 1$, (b) $\beta_M < 1$, and (c) $\beta_M > 1$.

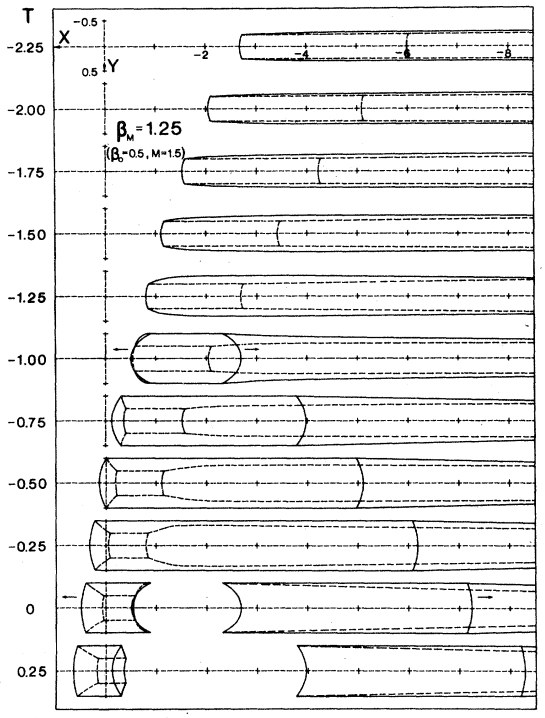

FIG. 8. Sequential, framed images of a travelling cube of side length $L_0=1$ with $\beta_M=1.25$.

ue β_M^e decreases to a value <1 at the rear face of the object so that, at some intermediate plane in the object, a value $\beta_M^e=1$ is realized. Exactly this case is illustrated in Fig. 8, where $\beta_0=0.5$, $\beta_M=1.25$, and, as for Fig. 7, $M=1.5$ and $L_0=1$. For Fig. 8, $\beta_M^e=1$ exactly at the midplane $z_0=-0.5$ so that points behind it have $\beta_M^e<1$, while $\beta_M^e>1$ for points in front of it. The resulting image behavior in time is one of the most bizarre yet. Thus, the back half of the object, with $\beta_M^e<1$, is visible for all times and forms only a single (causal) image while the front half of the object, with $\beta_M^e>1$, becomes visible only after some initial time and then produces two images which travel antiparallel to each other. At earlier times then, only the back half of the object is visible while, at later times, one complete image is visible along with a second, incomplete image describing only the front half of the object.

The imaging of a three-dimensional object gives rise to a new type of image distortion referred to as "longitudinal shearing," which is the distortion resulting from the object's finite depth along the optic axis of the imaging system. The effect of longitudinal shearing in the image can best be seen by carefully comparing Figs. 7(a) and 7(b). Thus, focusing attention solely on the front and back faces of the cube, it is observed in Fig. 7(b) that the back face is always seen to "lag" behind the front face by an amount well in excess of the perspective position. This is a result of the fact that, in the instantaneous image, the front and back faces, although recorded at the same instant in time in the focal plane, are in effect "seen" to correspond to quite different times in the object space since, because of the finitely longer time required for light from the back face to reach the image plane, this face is always "seen" at a time slightly earlier than that for the front face. The image is thus continuously sheared along its depth. Direct experimental confirmation of this longitudinal shearing effect has been given by Duguay and Mattick[3] who, using an optical-Kerr-effect shutter switched by the picosecond laser pulses from a Nd:glass laser, photographed two longitudinally displaced but identical ultrashort laser pulses in flight through a scattering medium.

VI. IMAGING OF TIME-DEPENDENT, STATIONARY OBJECTS

It would be seriously incorrect to leave the reader with the impression that the various phenomena described by this imaging theory apply only to moving objects. Rather, the theory here developed applies quite generally to any object, stationary or moving, having an intensity distribution which is time dependent. Thus Eq. (24) is valid for any time-dependent intensity distribution $I_0(x_0, y_0, z_0, t)$ and does not necessarily nor indeed explicitly involve any motion of the object in part or in whole. This section examines the time-dependent behavior of the image of a stationary object, where the definition of a "stationary object" is taken in its most general sense to include a collection of either related or unrelated "events" occurring at specific, fixed points in the object space. For simplicity, the analysis presented is one-dimensional only; the extension of these results to fully three-dimensional objects is straightforward.

Consider two points in the object plane, x_{01} and x_{02}, where "events" occur at the times t_{01} and t_{02}, respectively. Without any loss in generality, it may be assumed that event "1" occurs before event "2", i.e., $\Delta t_0=t_{02}-t_{01}\geq 0$. These events are then observed to occur, referring back to Fig. 1, at the image points $X_1=Mx_{01}/d$ and $X_2=Mx_{02}/d$ at the times $t_1=t_{01}+\tau(X_1)$ and $t_2=t_{02}+\tau(X_2)$, respectively. Thus the time difference between these two events as measured in the image plane is given by the expression

$$\Delta t=t_2-t_1$$
$$=\Delta t_0+[(M+1)d/Mc][(1+X_2^2)^{1/2}-(1+X_1^2)^{1/2}]\,. \quad (26)$$

Major errors in the interpretation of this measured time difference may occur whenever the two terms

on the right-hand side of Eq. (26) are comparable. Typical values of the second term (taking $X_2 = 0$ and $|X_1|$ in the range 0.1 to 0.5) vary from a few picoseconds to several hundred picoseconds, with even larger values when $M \ll 1$.

In general then, one must expect that $\Delta t \neq \Delta t_0$ whenever the second term on the right-hand side of Eq. (26) is comparable to Δt_0. However, one of the more serious errors which can arise is when the value of Δt becomes <0, i.e., the observed order of the two events is reversed. Clearly no such error is possible as long as $|X_2| > |X_1|$ since then the second term on the right-hand side of Eq. (26) must always be strictly >0 and so $\Delta t > \Delta t_0$. When $|X_2| < |X_1|$, however, this term is <0 and so $\Delta t < \Delta t_0$. To examine this behavior in more detail, the cases of causally related events and independent events are now considered separately.

A. Causally related events

In this case, some earlier event at x_{01} at time t_{01} causes some "effect" to occur at x_{02} at the later time $t_{02} > t_{01}$ by propagation of some signal from x_{01} to x_{02} with a velocity v_0 ($0 < v_0 \leq c$). Since Δt_0 is strictly >0 (assuming $x_{01} \neq x_{02}$), then one can calculate the ratio

$$\Delta t/\Delta t_0 = 1 - \beta_M \Delta_{12} = 1 - \beta_M \{[(1+X_1^2)^{1/2} - (1+X_2^2)^{1/2}]/|X_1 - X_2|\}, \tag{27}$$

where, as before, $\beta_M = (M+1)v_0/c > 0$. Note that the factor $\Delta_{12} > 0$ only if $|X_2| < |X_1|$. Thus, as long as $\beta_M < \Delta_{12}^{-1}$, $\Delta t/\Delta t_0 > 0$ (but, significantly, <1) and so the events are observed in the "correct" order (albeit "incorrectly" spaced in time). The special case where $\beta_M = \Delta_{12}^{-1}$ means that the events of "cause" and "effect" are observed to occur simultaneously in the image plane. However, when the inequality

$$\beta_M > \Delta_{12}^{-1} = \frac{|X_1 - X_2|}{(1+X_1^2)^{1/2} - (1+X_2^2)^{1/2}} \tag{28}$$

is satisfied, then $\Delta t/\Delta t_0 < 0$ and the "effect" is observed in the image plane to occur earlier than its "cause." Causal behavior is always the case, however, when $|X_2| > |X_1|$, with $\Delta t/\Delta t_0 > 1$. Note that, unlike the simpler case of a moving object considered previously where the nature of the image behavior was governed by the value of β_M being either <1, $=1$, or >1, the critical values of β_M deciding the exact nature of the temporal behavior of the image for a stationary object depend upon the value of Δ_{12}, i.e., upon the separation between the events as well as absolutely upon their positions.

B. Independent events

Consider first the case where Δt_0 is strictly >0. In this case, it is possible to define a purely ficticious velocity v_0^i (>0) as

$$v_0^i \equiv |x_{01} - x_{02}|/\Delta t_0, \tag{29}$$

where, since Δt_0 can be arbitrarily small, values of $v_0^i \gg c$ are permitted (v_0^i may be thought of as an imaginary propagation velocity for an imaginary signal linking the two independent events). The ratio $\Delta t/\Delta t_0$ is given by

$$\Delta t/\Delta t_0 = 1 - \beta_M^i \Delta_{12}, \tag{30}$$

where Δ_{12} is exactly as defined before in Eq. (27) and $\beta_M^i = (M+1)v_0^i/c > 0$. So, as was the case for causally related events, there exists three distinct possibilities whenever $|X_2| < |X_1|$: (1) $\beta_M^i < \Delta_{12}^{-1}$ gives $\Delta t/\Delta t_0 > 0$ and the observed temporal order of the two events in the image is the same as that in which they occurred in the object, (2) $\beta_M^i = \Delta_{12}^{-1}$ gives $\Delta t/\Delta t_0 = 0$ so that the events are observed to occur simultaneously in the image plane, and (3) $\beta_M^i > \Delta_{12}^{-1}$ yields $\Delta t/\Delta t_0 < 0$ and the events are observed in the image plane in a temporal order, which is reversed to their original occurrence in the object. When $|X_2| > |X_1|$, then $\Delta t/\Delta t_0$ is always >1 and tem-

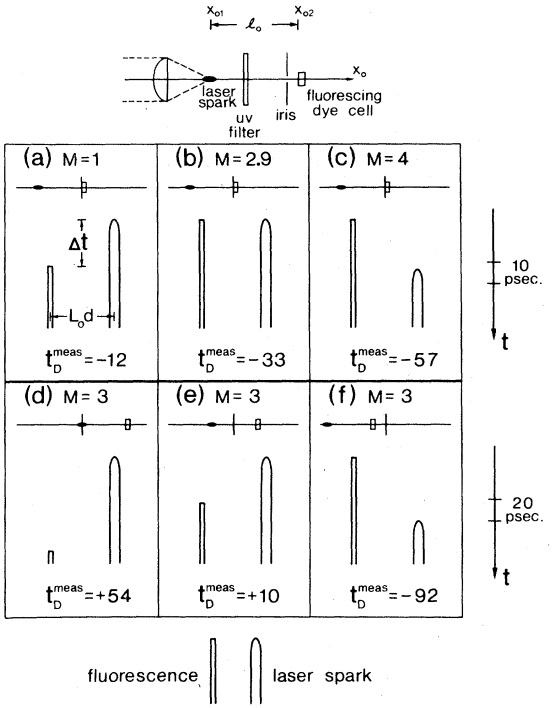

FIG. 9. Calculated images of the results of the experimental measurement of the delay time in the fluorescence induced by the radiation from a laser produced spark.

poral ordering is preserved in the imaging. The special case of $\Delta t = 0$ must be examined with the aid of Eq. (26). Thus, when $|X_2| < |X_1|$, the event at X_2 is seen earlier in the image plane while, when $|X_2| > |X_1|$, the event at X_1 is observed first.

To dramatically illustrate these temporally distorting effects in the imaging of a stationary object, Fig. 9 shows the results of a hypothetical one-dimensional experiment. Here, an ultrashort laser pulse is focused in air to produce a laser spark and the uv radiation from this spark is then observed to induce fluorescence in a cell situated at a distance l_0 from the spark. The experimental objective is to measure, using a high-speed streak camera, the delay time between the initiation of the spark and the onset of the fluorescence after allowing for the transit time of l_0/c, i.e., the measured delay time will be given by $t_D^{\text{meas}} = \Delta t - (l_0/c)$. In calculating Fig. 9, an actual delay time of 10 psec ($= 0.3 l_0/c$) has been assumed and the parameter d_0 has been fixed throughout. The top three results shown in Fig. 9 have identical values of x_{01} and x_{02} with M as a variable while the bottom three results have a constant magnification M but varying values for x_{01} and x_{02} (subject, of course, to the requirement $l_0 = |x_{01} - x_{02}|$). In particular, the reader's attention is drawn to the two extreme right-hand results, where the condition $\beta_M > \Delta_{12}^{-1}$ is satisfied and thus where the induced fluorescence caused by the laser spark is in fact observed to occur before the initiation of the spark! Furthermore, as Figs. 9(a) and 9(b) illustrate, a negative delay time is measured whenever the parameter Δ_{12} of Eq. (27) is >0 since, even though the ratio $\Delta t/\Delta t_0$ may be >0, the difference $\Delta t - \Delta t_0$ is <0 by virtue of the fact that $\Delta t/\Delta t_0$ is <1. In Fig. 9(f), the image of the fluorescing cell lies at the point X_{int} given in Eq. (12).

VII. DISCUSSION

The theory presented in this paper pertains to the *instantaneous* appearance of the image in the *focal plane* of the imaging system, features which deserve further examination in light of practical, high-speed photographic devices. Firstly, the instantaneous image description is only realized in practice when the resolution time of the photographic system (e.g., the temporal resolution of a streak camera or the exposure time of an optical-Kerr-effect shutter) is $\ll$ the temporal duration of the object. When this is not strictly the case, then Eq. (24) must be generalized to include a time integration as

$$I_i(x, y, t) = \frac{K_3}{t_s} \int_{t-\frac{1}{2}t_s}^{t+\frac{1}{2}t_s} \int_{-\infty}^{\infty} I_0 \{x/M_e(z_0), y/M_e(z_0), z_0, t' - \tau(x, y, z_0)\}\, dZ_0 dt' , \tag{31}$$

where t_s represents the resolution or "shutter" time of the photographic system and $M_e(z_0)$ is given by Eq. (23). Similarly, for the two-dimensional case, the generalization of Eq. (21) is

$$I_i(x, y, t) = \frac{K_2}{t_s} \int_{t-\frac{1}{2}t_s}^{t+\frac{1}{2}t_s} I_0(x/M, y/M, t' - \tau(x, y))\, dt' . \tag{32}$$

Hence note that, in the original instantaneous image equations, the transmission constants K_2 and K_3 incorporated this shutter time t_s as an implicit factor. A finite t_s which is $\gtrsim$ the object's temporal duration means, of course, that the image described by either Eqs. (31) or (32) must be "blurred" or "smeared" in time in comparison to the ideal case of the framed, instantaneous image described by either of Eqs. (24) or (21). The second feature of the theory presented here is that the image is temporally resolved or defined in the focal plane of the imaging system. Although this is exactly the case for most streak-camera systems[9-11] and for the focal plane version of the optical-Kerr-effect shutter,[5-8] consideration must be given to other systems where the shuttering or time resolving plane lies somewhere between the focal and object planes.[1-4] It suffices to say, qualitatively, that as the shuttering plane is moved away from the focal plane of the lens towards the object plane, the observability of the various distorting phenomena described in this paper decreases monotonically. Indeed, in the limit where the shuttering plane coincides with the object plane, all such distorting effects in the image and anticausal features vanish exactly since, in this limit, the image would be formed by light which leaves the object simultaneously (as opposed to light which reaches the focal plane simultaneously) and so must necessarily be exactly faithful.

The many illustrations given in this paper of the instantaneous images and their evolution in time for various objects have served to concretely establish the importance and the magnitude of the distortions which can arise. Conversely, these illustrations also serve to establish those criteria which, when met, would result in essentially distortion-free, faithful photography. Clearly, the obvious parameter of principal importance is the val-

ue of β_M since, if its value was at the control of the experimenter, the realization of a $\beta_M \ll 1$ would in itself be sufficient to ensure distortionless imaging (imperfections in the optics aside). When this is not the case, then it is still possible to obtain largely distortion-free instantaneous images by ensuring that the transverse extent and particularly the longitudinal depth are negligibly small in comparison to d/M. Of course, even though the individual instantaneous images would be faithful, a finite β_M value would still result in the motion of the object as a whole being highly nonlinear, viz., Fig. 6. In any event, as indicated previously in the paper, best results are generally obtained when the object, stationary or otherwise, is photographed exactly when it is centered about the optic axis of the imaging system.

An important consideration, in those cases where some degree of image distortion is unavoidable, concerns the "invertibility" of the recorded image to give a faithful reconstruction of the object. Strictly speaking, a unique and true reconstruction of the object from a knowledge of the instantaneous image and its temporal behavior is only possible if, (i) the object is strictly two- (or one-) dimensional and, (ii) the image recorded is truly an instantaneous image ($t_s \ll$the object's duration). This, of course, is the case described by the imaging Eq. (21). Either the presence of some finite longitudinal depth in the object or the fact that the recorded image is not a truly instantaneous one ($t_s \gtrsim$ the object's duration) would mean that the image is no longer uniquely invertible so that the object's profile, position, and temporal variation cannot be exactly or uniquely reconstructed from a knowledge of the image alone. This is the case when one of Eqs. (24), (31), or (32) is applicable. Practically speaking, however, some degree of this "loss of information" resulting from a finite object depth or a finite resolution time is tolerable, which still permits a reasonably faithful image-to-object reconstruction. In this regard, note is here made of an alternate imaging design which would ensure distortionfree imaging for all β_M values and object profiles. Specifically, if the image and object "planes" (see Fig. 4) where spherical rather than planar, with radii of curvature of d and d_0, respectively, and concentric with the midpoint of the lens, then the optical path length in such a system would be a constant for all object-to-image conjugate points. Hence all distortions due to transit time differences would vanish exactly. Even if only the image space were spherical, then, provided M was not too small, the degree of distortion which could arise would be greatly reduced.

Care has been taken throughout the paper to avoid any reference to the various phenomena described as "relativistic" since, because the observability of these phenomena is governed by the enhanced parameter $\beta_M = (M+1)\beta_0$, it is possible to observe these effects even in the case where $\beta_0 \ll 1$, provided that the magnification M is sufficiently large. Of course, there will generally exist practical limitations to the size of M set by the finite dimensions of the object. Nevertheless, in some situations, for example the current work on x-ray streak photography of laser imploded microballoons, large values of M ($\simeq 50$) are commonly employed[20] and special attention must be given to the possible occurrence of non-negligible values of β_M.

A final point to be raised concerns the use of the term anticausal. Objections may be raised to its use on the grounds that, although the image can exhibit time reversal and hence exhibit "apparent" anticausality, the real situation concerning the temporal behavior to the real object must be causal. To answer this objection, it is necessary to reexamine the nature of the image–object relationship in general. In the vast majority of cases, $\beta_M \ll 1$ and the object-to-image relationship is unique, straightforward, and, in some senses, trivial. So much so, in fact, that this relationship is invariably ignored and one unconsciously speaks of the object directly from a knowledge of the image without the need to explicitly consider the image-to-object "inversion." This paper has shown, however, certainly in those cases where β_M is finite, that the image-to-object relationship is a complicated one resulting in images which often bear little if any resemblence to the object they describe. One is thus no longer able to unconsciously equate image and object as faithful reproductions of one another but, rather, must treat the image as a principal entity apart from (albeit related to) the object. In short, the only real, directly observable entity is the recorded image itself, from which a knowledge of the object must then be derived. Thus, in this sense, anticausal behavior is a real, observable phenomenon occurring in a real, observable image; it is subject to demonstration and measurement just an any other physical phenomenon. There is, however, *no* contradiction with the axioms of relativity since the correct interpretation of the image, according to the theory presented in this paper, guarantees that the object's behavior must always be strictly causal.

ACKNOWLEDGMENTS

The author wishes to express his deep appreciation to Dr. M. C. Richardson of the Division of Physics, The National Research Council of Canada,

under whose supervision this work was initiated. Helpful discussions with Dr. René Serov of the Lebedev Institute, Moscow, concerning initial attempts to analytically solve the problem of a moving-point-source object are also warmly acknowledged. The author gratefully acknowledges support from a NATO postdoctoral fellowship.

APPENDIX: ANALYSIS FOR A FINITELY THICK LENS

The nonlinear motion and the distortion of the image described in this paper are the result of small differences in the transit time of the light travelling from the object to the image plane. For the perfect, thin lens, these transit time differences from different points in the object depend only upon the geometry of the imaging system (i.e., upon d and d_0 only). For any real, finitely thick lens, however, there will exist small, second-order transit time differences arising in the optical-path length through the lens itself. By reexamining the image motion of a travelling point source object for an imaging system employing a simple "thick" lens, this appendix calculates these second-order corrections to the "thin-lens solutions" of the text and shows that, quite generally, the "thick-lens solutions" are essentially identical.

The simple, thick-lens model adopted here is that of a symmetrical, biconvex lens and illustrated in Fig. 10. With a central lens thickness of δ and a focal length of f, the (maximum) aperture radius of the lens is

$$r^2 = 2(n-1)f\delta - \tfrac{1}{4}\delta^2 , \tag{33}$$

where n is the refractive index of the lens substrate (the object and image spaces are assumed to have a refractive index of unity). Fermat's theorem applied to the thick lens still ensures that all possible paths from the conjugate object-to-image points $x_0 = x/M$ to X through the lens have identical optical-path lengths so that, for the purposes of calculating the optical-path-length function $s(R, X)$ for the thick lens, any of the various "rays" may be used. The simplest choice is that of the ray which just intersects the lens at its edge where the lens thickness may be taken as infinitesimal (the solid line in Fig. 10). From this, the optical path length from $x_0 = x/M$ to x is readily found to be

$$s(R,X) = (d/M)\{[1+(MR-X)^2]^{1/2} + M[1+(R+X)^2]^{1/2}\} , \tag{34}$$

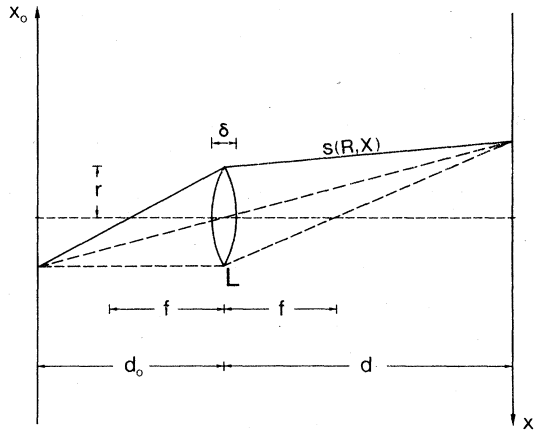

FIG. 10. Parameters and optical path lengths for an imaging system employing simple, "thick," symmetrical biconvex lens.

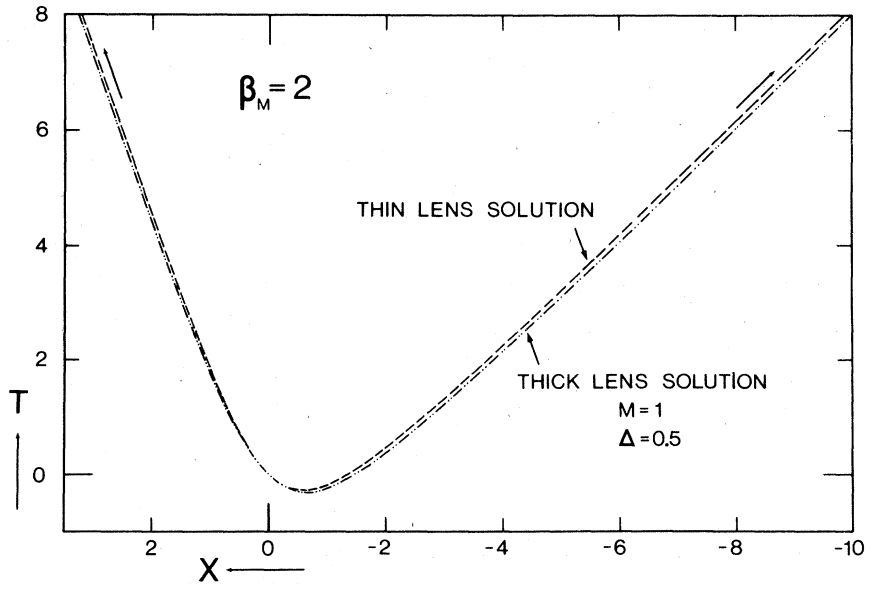

FIG. 11. Motion of a travelling-point-source object with $\beta_M = 2$ as calculated with the thin-lens solution and with the thick-lens solution using the "worst case" parameters of $\Delta = 0.5$ and $M = 1$.

where $X = x/d$ and R is the dimensionless lens "radius"

$$R^2 = r^2/d^2 = [2(n-1)\Delta - \tfrac{1}{4}\Delta^2]/(M+1)^2 \qquad (35)$$

with $\Delta = \delta/f$.

The position of the point source object is given by the equation of motion

$$x_0(t) = v_0 t + v_0 s(R, 0)/c\,, \qquad (36)$$

whence, using Eq. (2), the point image is found to obey the equation

$$T = X + [M\beta_M/(M+1)]\{[1+(R+X)^2]^{1/2} - [1+R^2]^{1/2}\} + [\beta_M/(M+1)]\{[1+(MR-X)^2]^{1/2} - [1+M^2R^2]^{1/2}\}\,, \qquad (37)$$

which may be compared with the analogous thin-lens Eq. (4). The image motion $X(T)$ was calculated from Eq. (37) for the values $\beta_M = 0.5$, 1, and 2 and for different values of M, with various values for the lens thickness as large as $\Delta = 0.5$. These thick lens solutions were then compared directly to the thin lens solutions plotted in Fig. 2(a). It was found that discernable differences between the two solutions occurred only for the largest Δ values and then only in the off-axis regions $|X| \gtrsim 1$. To illustrate, Fig. 11 shows the motion of a traveling point source object with $\beta_M = 2$ calculated with the thin-lens solution, Eq. (11), compared to that calculated with the thick-lens solution, Eq. (37). Moreover, Fig. 11 represents a "worst case" example with a lens thickness equal to one-half of its focal length and a magnification $M = 1$ chosen to maximise the difference between the solutions. The differences in the near-axis regions, $|X| \ll 1$, were always negligible. This finding is also substantiated analytically by approximating Eq. (37). Thus, labelling the $T(X)$ solution to Eq. (37) as T_t to distinguish it from the $T(X)$ solution to Eq. (4), one finds, to second order in R^2,

$$T_t - T \simeq -0.5MR^2\beta_M[1-(1+X^2)^{-1/2}] \qquad (38)$$

for which it is noted that the maximum value of MR^2 occurs at $M = 1$ whence

$$MR^2|_{\max} = r^2/4f^2 = 1/16F^2\,,$$

where $F = f/2r$ is the f number of the lens [for the maximum aperture given by Eq. (33)]. Calculations with Eq. (38) show that, for any value of β_M, the relative difference between the thick-lens and the thin-lens solutions at any point X is always <1% as long as the f number of the lens is >1.

---

*Present address: Lash Miller Chemical Laboratories, Univ. of Toronto, 80 St. George St., Toronto, Ontario, Canada M5S 1A1.

[1]M. A. Duguay, in *Progress in Optics* (North-Holland, New York, 1976), edited by E. Wolf, Vol. 14, pp. 161–193.

[2]M. A. Duguay and J. W. Hansen, IEEE J. Quantum Electron. QE-7, 37 (1971); J. W. Hansen and M. A. Duguay, J. Soc. Motion Pict. Telev. Eng. 80, 73 (1971).

[3]M. A. Duguay and A. T. Mattick, Appl. Opt. 10, 2162 (1971).

[4]G. C. Vogel, A. Savage, and M. A. Duguay, IEEE J. Quantum Electron, QE-10, 642 (1974).

[5]K. Sala, Masters thesis (Carleton University, Ottawa, Canada, 1973) (unpublished).

[6]M. C. Richardson and K. Sala, Appl. Phys. Lett. 23, 420 (1973).

[7]A. N. Rubinov, M. C. Richardson, K. Sala, and A. J. Alcock, Optics Commun. 12, 188 (1974); Appl. Phys. Lett. 27, 358 (1975).

[8]K. Sala and M. C. Richardson (unpublished).

[9]M. Ya. Schelev, M. C. Richardson and A. J. Alcock, Appl. Phys. Lett. 18, 354 (1971); M.C. Richardson, IEEE J. Quantum Electron QE-9, 768 (1973).

[10]D. J. Bradley, B. Liddy, and W. E. Sleat, Opt. Commun. 2, 391 (1971). Also see the review by D. J. Bradley and G. H. C. New, Proc. IEEE 62, 313 (1974).

[11]S. D. Fanchenko and B. A. Frolov, Pis'ma Zh. Eksp. Teor. Fiz. 16, 147 (1972) [JETP Lett. 16, 101 (1972).]

[12]R. Penrose, Proc. Cambr. Philos. Soc. 55, 137 (1959).

[13]J. Terrell, Phys. Rev. 116, 1041 (1959).

[14]An earlier treatment of this subject which has apparently gone unnoticed was given by W. H. McCrea, Sci. Proc. R. Dublin Soc. 26, 27 (1952).

[15]See the reviews and references therein by N. G. McGill, Contemp. Phys. 9, 33 (1968); P. M. Mathews and M. Lakshmanan, Il Nuovo Cimento 12B, 168 (1972); Ya. A. Smorodinskii and V. A. Ugarov, Usp. Fiz. Nauk. 107, 141 (1972) [Sov. Phys. Usp. 15, 340 (1972)].

[16]Of these two parameters, x_{int} is the "better" one since it is an intrinsic parameter of the imaging system dependent only upon β_M, while T_{int} depends upon the somewhat arbitrary choice of time origin as set by the equation of motion of the object.

[17]All references to object shape and length are those of the object in motion as described in the stationary, object space coordinate frame of the imaging system. For material objects in motion, this shape differs from its rest shape by a simple Lorentz contraction along that direction parallel to the motion. The theory presented in this paper deals only with the imaging transformation of the "objective shape" of the object (i.e., its shape described in the stationary coordinate frame) into an instantaneous image and, thus, the equations derived are valid quite generally for any object, material or otherwise, in motion or stationary. As such, the theory given here is completely independent of any relativistic considerations and the only way in which relativity theory can enter in at all is through the distinct and here implicit step of a Lorentz contraction of a material object in motion. A more detailed discussion of the delineation of the relativistic and imaging effects is given by Mathews and Lakshmanan in Ref. 15.

[18]Note, in theory, that a faithful image can be obtained for any values of β_M and L_0 provided the entire image lies completely in either of the far off-axis regions

$|X| \gg 1$. Realistic limitations, however, on any practical lens would largely rule out any use of the regions $|x| \gg d$ and so this possibility is ignored in the present analysis.

[19]In particular, no account is explicitly given of the anisotropy in the emitted radiation or of the Doppler shifting of this light when $\beta_0 \sim 1$. Again, such relativistic effects alter only the relative intensity distribution or the spectral variation within the image and not its spatial profile or extent. See, e.g., H. Muirhead, *The Special Theory of Relativity* (MacMillan, New York, 1973), pp. 42–47, 69–75.

[20]See e.g., The Lawrence Livermore Laboratory Laser Program Annual Report, 1976 (UCRL-50021-76), pp. 3–68, 3–69 (unpublished).